Hard convex lens-shaped particles: Densest-known packings and phase behavior

Giorgio Cinacchi[1,a)] and Salvatore Torquato[2,b)]
[1]*Departamento de Física Teórica de la Materia Condensada, Instituto de Física de la Materia Condensada (IFIMAC), Instituto de Ciencias de Materiales "Nicolás Cabrera," Universidad Autónoma de Madrid, Campus de Cantoblanco, E-28049 Madrid, Spain*
[2]*Department of Chemistry, Department of Physics, Institute for the Science and Technology of Materials, Program for Applied and Computational Mathematics, Princeton University, Princeton, New Jersey 08544, USA*

(Received 14 October 2015; accepted 12 November 2015; published online 14 December 2015)

By using theoretical methods and Monte Carlo simulations, this work investigates dense ordered packings and equilibrium phase behavior (from the low-density isotropic fluid regime to the high-density crystalline solid regime) of monodisperse systems of hard convex lens-shaped particles as defined by the volume common to two intersecting congruent spheres. We show that, while the overall similarity of their shape to that of hard oblate ellipsoids is reflected in a qualitatively similar phase diagram, differences are more pronounced in the high-density crystal phase up to the densest-known packings determined here. In contrast to those non-(Bravais)-lattice two-particle basis crystals that are the densest-known packings of hard (oblate) ellipsoids, hard convex lens-shaped particles pack more densely in two types of degenerate crystalline structures: (i) non-(Bravais)-lattice two-particle basis body-centered-orthorhombic-like crystals and (ii) (Bravais) lattice monoclinic crystals. By stacking at will, regularly or irregularly, laminae of these two crystals, infinitely degenerate, generally non-periodic in the stacking direction, dense packings can be constructed that are consistent with recent organizing principles. While deferring the assessment of which of these dense ordered structures is thermodynamically stable in the high-density crystalline solid regime, the degeneracy of their densest-known packings strongly suggests that colloidal convex lens-shaped particles could be better glass formers than colloidal spheres because of the additional rotational degrees of freedom. [http://dx.doi.org/10.1063/1.4936938]

I. INTRODUCTION AND MOTIVATION

Systems of hard particles are of interest in a variety of scientific fields. To find the densest, optimal, packing of a collection of hard non-space-filling particles is a basic, long-standing problem in mathematics.[1–5] The study of hard-particle systems is also very relevant to condensed matter physics[6] and materials science.[7,8] In fact, short-range steeply repulsive intermolecular interactions are primarily responsible for determining the stability and structure of a molecular system in condensed states of matter (crystalline,[9,10] glassy,[11] liquid-crystalline,[12] liquid[13,14]), while hard-particle interactions are well-approximated experimentally by colloidal[15] particles, now synthesizable of various shapes and sizes.[16–18]

The three-dimensional hard sphere is the most basic hard-particle model. Many aspects of this model system have been studied and the literature on the subject is vast.[13,14,19–21] The fact that a hard-sphere system possesses a disorder-order, fluid-crystal phase transition was remarkably hypothesized[22] and then demonstrated in the earlier applications of numerical simulation techniques.[23,24] The co-existence density and pressure values were subsequently evaluated by free-energy calculations.[25] Interest then moved toward the high-density regime where metastable fluid and glassy states and a stable crystal phase exist. Investigations on the metastable fluid and glassy states[26] progressively led to the introduction of the concept of maximally random jammed state.[21,27] Investigations on the crystal phase concluded that the face-centered-cubic (fcc) crystal is thermodynamically stable (by a very slight amount) over the hexagonally close-packed (hcp) crystal.[28,29] These crystals are two of the infinitely degenerate (Barlow) stacking variants that provide the hard-sphere densest packings. That there is no packing arrangement of congruent hard spheres that fills three-dimensional Euclidean space more densely than the fcc lattice was conjectured by Kepler and mathematically proved only recently.[30]

Comparatively much less is known about dense packings, equilibrium phase behavior, and non-equilibrium glassy states of hard non-spherical particle systems. There are many ways to generalize the hard sphere to hard non-spherical particle models, e.g., ellipsoids,[31–39] spherocylinders,[40–44] cut-spheres,[45,46] polyhedra,[47–58] and *superballs*, a shape that interpolates between the cube and the octahedron via the sphere.[59] Together with all these hard convex particle models, increasing attention is also being paid to hard non-convex particle models such as bent-shaped particles,[60] (hollowed) spherical caps,[61] helices,[62] and tori.[63]

This work addresses dense ordered packings and equilibrium phase behavior of monodisperse systems of

a)Electronic mail: giorgio.cinacchi@uam.es
b)Electronic mail: torquato@princeton.edu

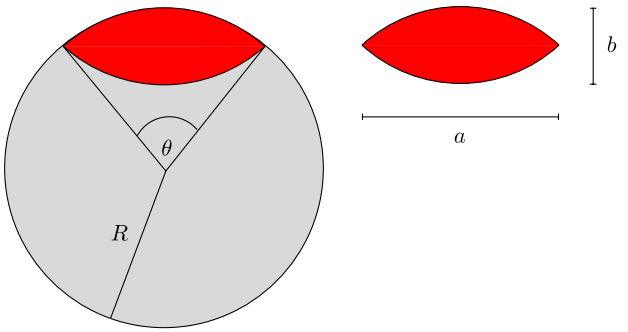

FIG. 1. (Left) Hard convex lens-shaped particle (red or dark gray region) and its parent sphere (the particle plus the complementing light gray region), with radius R and opening angle θ. (Right) Definition of the major, a, and minor, b, axes, with the aspect ratio defined as $\kappa = b/a$.

hard convex lens-shaped particles. These centrally symmetric discoidal particles are defined by the volume common to two intersecting congruent spheres. In Fig. 1, a side view of a particle of this type is given, together with the definition of a few relevant quantities: the opening angle, θ, the major and minor axes, $a = 2R\sin\frac{\theta}{2}$ and $b = 2R\left(1-\cos\frac{\theta}{2}\right)$. The aspect ratio is defined as $\kappa = b/a$: it takes on values in the interval [0,1], with zero corresponding to the limit of the hard infinitesimally thin disk and unity corresponding to the limit of the hard sphere.

These hard particles, simply called lenses henceforth,[64] were originally introduced to model monolayers of discotic liquid-crystal molecules.[65] They are of current interest for several reasons. They are yet another generalization of the hard-sphere model, not dissimilar from hard oblate ellipsoids (Fig. 2). In contrast to an ellipsoid though, a lens is not an affine transformation of a sphere. Moreover, the surface of lenses possesses both regions that are smooth (continuous radius of curvature) and non-smooth cusps, features that make them particularly interesting to study. Indeed, it is not clear how these facts influence their dense packing arrangements and phase behavior and then how similar these are to the dense packing arrangements and phase behavior of hard oblate ellipsoids. Dense disordered packings of lenses, among other hard axisymmetric particles, have been recently studied using a mean-field theory.[66] It would be of interest to test the predictions made there: a knowledge of dense ordered packings and equilibrium phase behavior is a pre-requisite for such a study. Given today's developments in colloidal particle synthesis, we envision that colloidal lenses could be readily produced.[67] This capability would offer a testbed for corresponding theoretical and computational studies.

In Sec. II, we present several analytic constructions of dense crystalline packings of lenses. Two of these analytically constructed dense crystalline packings are subsequently used as starting configurations for a series of Monte Carlo[68] (MC) numerical simulations aimed at checking their mechanical stability at finite pressure and then sketching the phase diagram as a function of κ. These MC calculations are discussed in Secs. III and IV A. The MC method is also employed in Secs. III and IV B to improve on the value of the close packing density. These numerical simulations finally guide us, in Sec. VI, toward analytic constructions of the densest-known

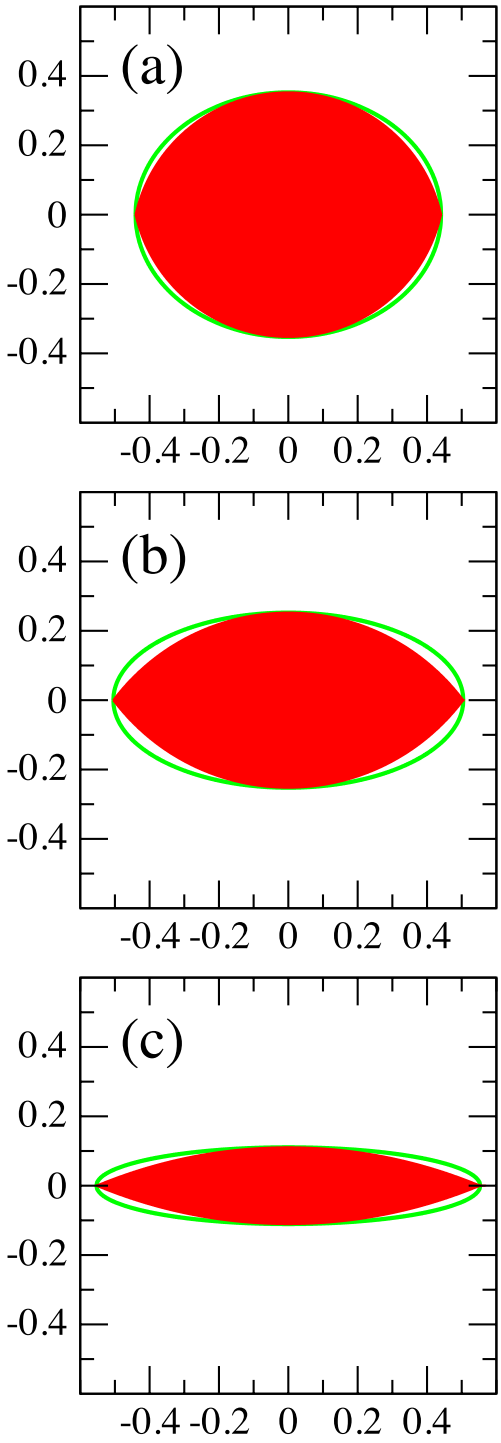

FIG. 2. Side view of a lens (red or dark gray region) compared to that of an oblate ellipsoid (interior of the green or light gray curve) with the same values of a and b for $\kappa = 0.8$ (a), $\kappa = 0.5$ (b), and $\kappa = 0.2$ (c).

packings of lenses. Sec. VI provides concluding remarks on our work and an outlook for future research avenues.

II. DENSE PACKING CONSTRUCTIONS

In looking for candidates for the densest packings of lenses, we focus on crystalline packings since all evidence strongly suggests that noncrystalline packings can never be the densest in low (<4) dimensions. It is useful to first recall what is known about hard spheres, corresponding to

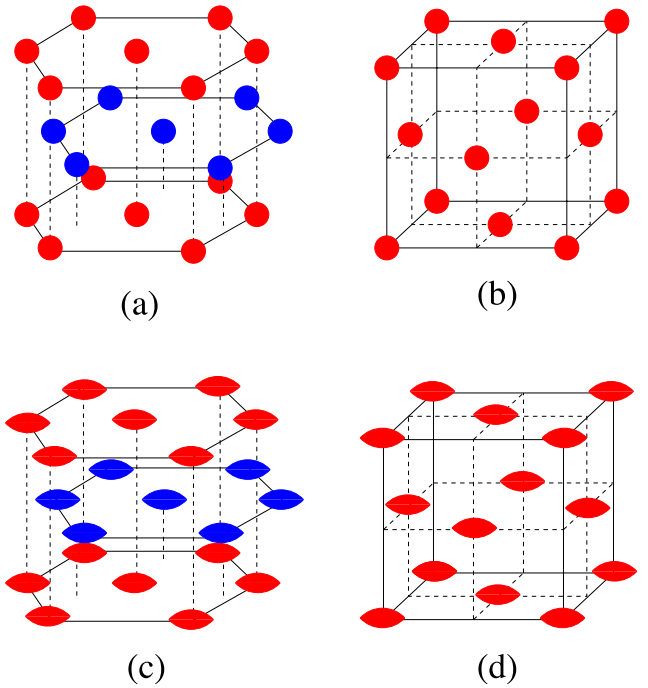

FIG. 3. Schematic pictures of: (a) the hcp crystal for hard spheres, (b) the fcc crystal for hard spheres, (c) the hcp-like crystal for lenses, (d) the fcc-like crystal for lenses.

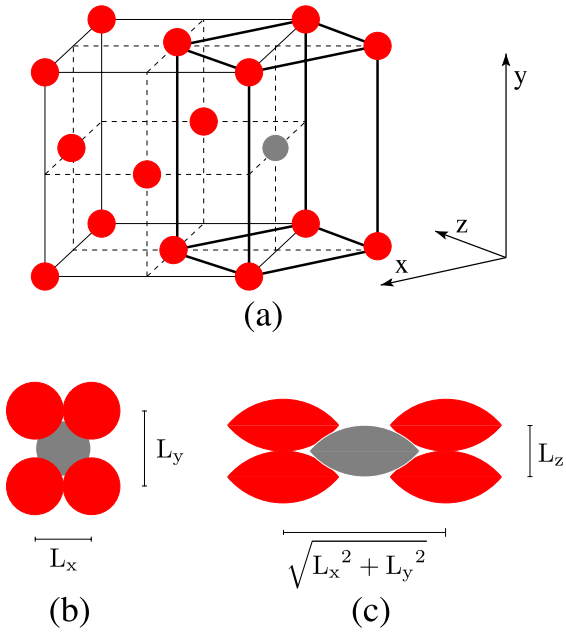

FIG. 4. (a) Schematic picture of a Bain transformation that regards a fcc crystal of hard spheres as a special bco crystal formed by those particles at the vertices of the cuboid with thicker edges together with the gray particle at its center. In a bco-like crystal, the lenses are oriented along the direction [110], i.e., the axis labelled as z; a schematic picture of this crystal of lenses is given as viewed from the top (b) and diagonally (c), with L_k the length of the unit cell along the k axis.

lenses in the limit $\kappa = 1$. The hard-sphere densest packing is given by the fcc crystal along with all its (Barlow) stacking variants, including the hcp crystal. In Figs. 3(a) and 3(b), the hard-sphere hcp and fcc crystals are schematically shown. Based on these results for hard spheres, the following five dense packings of lenses have been constructed:

1. hcp-like crystal: This construction is obtained by replacing each hard sphere in the hcp crystal with a lens while orienting its main (C_∞) symmetry axis along the direction perpendicular to the triangular-lattice layer planes and then optimizing particle contacts by suitably varying the unit cell shape and size. This hcp-like crystal is schematically shown in Fig. 3(c).
2. fcc-like crystal: This construction is obtained by replacing each hard sphere in the fcc crystal with a lens while orienting its C_∞ symmetry axis along the [001] direction and then optimizing particle contacts through suitably changing the unit cell shape and size. In this way, a fcc-like crystal is generated, as schematically shown in Fig. 3(d).
3. bco-like crystal: This construction uses a Bain transformation[70,71] that views the fcc crystal of hard spheres as a special body-centered-orthorhombic (bco) crystal [Fig. 4(a)]. Each sphere is replaced by a lens oriented along the [110] direction, i.e., the z axis in Fig. 4(a), and particle contacts are then optimized by suitably varying the unit cell shape and size. This bco-like crystal is schematically shown in Figs. 4(b) and 4(c).
4. elo-like crystal: Here we exploit the apparent similarity that lenses bear with oblate ellipsoids and assume that the former will pack as the latter do in their laminated orthorhombic (elo) crystal.[35] This crystal is related to the layering structure of the hard-sphere fcc crystal. In this packing, if $1/\sqrt{3} \le \kappa \le 1$, oblate ellipsoids in two adjacent layers have mutually orthogonal orientations, the ones in one layer having their C_∞ axes along the [100] axis and the others in the next layer having them along the [010] axis; if $\kappa \le 1/\sqrt{3}$, the angle between the major (minor) axes of two oblate ellipsoids in two adjacent layers progressively diminishes until it vanishes in the hard-infinitesimally thin-disk limit. This two-particle basis crystal is the densest-known packing for ellipsoids.[35] Since an oblate ellipsoid has a larger volume than a lens having the same values of a and b (Fig. 2), the elo structure itself cannot be optimal for lenses, since the density can be increased by optimizing particle contacts through changing the fundamental cell shape and size even while keeping the lenses in the same orientation as that of oblate ellipsoids. The resulting crystal is denoted elo-like (Fig. 5).
5. bco2-like crystal: This construction is based on combining aspects of previous two constructions. Following the example of oblate ellipsoids and their propensity to arrange layer-by-layer perpendicularly for $1/\sqrt{3} \le \kappa \le 1$, one can take the aforementioned bco-like crystal and change the orientation of the central lens so that it lies orthogonal to the others and oriented along the x axis in Fig. 4(a) and then optimize particle contacts by changing the fundamental cell shape and size. This two-particle basis crystal is denoted bco2-like.

In Fig. 6, the dependence of the packing fraction $\phi = \varrho v$, with ϱ the number density and v the particle volume,[72] on κ is reported for the five aforementioned dense packing constructions. The hcp-like crystal shows an undesirable trend of ϕ monotonically decreasing with decreasing κ. This trend

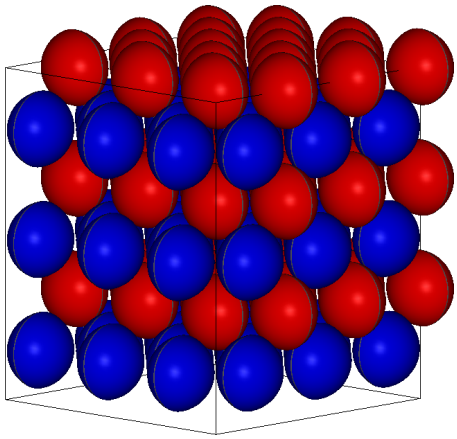

FIG. 5. Image of the elo-like crystal for lenses, in the case the value of the aspect ratio κ is sufficiently close to unity. In that case, particles belonging to two adjacent layers are arranged perpendicularly (which is motivated by the construction of the densest-known packing of ellipsoids[35]) and colored differently. Image was created with the program QMGA.[69]

is also exhibited by the fcc-like crystal but only for $\kappa \gtrsim 0.873$. For smaller value of κ, its value of ϕ increases and gets closer and closer to that for the bco-like crystal. The latter shows the desired trend of ϕ monotonically increasing with decreasing κ. For the elo-like structure in the regime of larger κ, optimizing the fundamental cell dimensions, thus obtaining a packing denser than that one would have by just replacing each oblate ellipsoid with a lens, is not enough to remove the undesirable trait of having hard convex non-spherical particles that pack less densely than hard spheres do (the opposite of the Ulam conjecture,[73] for which a first mathematical proof has appeared very recently for the special case of a centrally symmetric convex particle that is very nearly spherical in shape[74]). This monotonically decreasing trend stops at $\kappa \sim 0.714$, the corresponding value of ϕ for the elo-like structure having a local minimum. For smaller values of κ, the value of ϕ increases until $\kappa = \Phi - 1 = 1/\Phi$, with Φ the golden section.

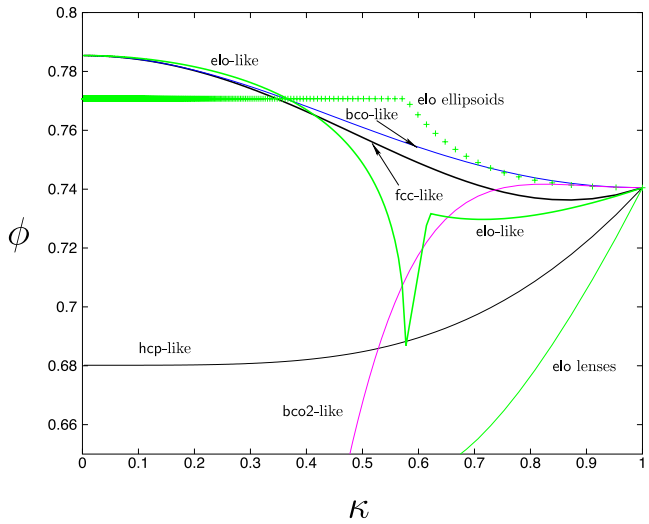

FIG. 6. Packing fraction ϕ as a function of the aspect ratio κ for the five different dense crystalline packing constructions of lenses: hcp-like (thin black line), fcc-like (black line), bco-like (blue line), elo-like (green line), bco2-like (magenta line). For comparison, the behavior of ϕ versus κ for the unoptimized elo crystal (thin green line) and for the elo crystal of oblate ellipsoids (green crosses) is also shown.

Then, it drops suddenly until $\kappa = 1/\sqrt{3}$. For smaller values of κ, the increasing trend is recovered thanks to the two particles of the basis progressively becoming more aligned with respect to one another. In this way, the elo-like structure ends up, for $\kappa \lesssim 0.373$, to slightly surpass in packing fraction the bco-like crystal. Then, both reach the same limiting value of ϕ as the hard-infinitesimally thin-disk limit is approached. Concerning the bco2-like crystal, while showing a behavior very similar to that of the bco-like crystal for large enough values of κ (a fact suggesting a certain degeneracy in the attainable values of ϕ at least in the vicinity of $\kappa = 1$), its packing fraction expectedly drops suddenly as the lenses become more anisometric.

It is instructive to compare the packing fractions of oblate ellipsoids in their densest-known packing to the largest packing fractions of lenses among the five reported thus far as a function of κ: Lenses pack slightly more densely when $0.733 \lesssim \kappa < 1$; but they fill three-dimensional Euclidean space less efficiently than oblate ellipsoids do when $0.366 \lesssim \kappa \lesssim 0.733$; finally they pack increasingly more densely when $\kappa \lesssim 0.366$; see Fig. 6 for a numerical comparison. While lenses and oblate ellipsoids appear to be similar in shape, their corresponding dense crystalline packing fraction trends can be quite different. Note that the packing fraction of oblate ellipsoids of any aspect ratio in the hcp-, fcc-, and bco-like crystal arrangements coincides with the hard-sphere fcc crystal packing fraction, $\phi_{\text{fcc}} = \dfrac{\pi}{3\sqrt{2}}$. Indeed, parallel ellipsoids can be obtained from spheres by an affine, packing fraction preserving, transformation. That this affine transformation holds was what led to the belief that the fcc-like crystal was the densest for freely rotating ellipsoids until it was recently shown that these particles can take advantage of their rotational degrees of freedom and actually pack more densely in the laminated crystal with a fundamental cell of two non-parallel particles.[35] Lenses are not an affine transformation of spheres though and the packing fraction of hcp-, fcc-, and bco-like crystals exhibits a different trend with κ. This might be at the root of lenses not requiring, unlike ellipsoids, a drastic change in their orientation to achieve a crystalline packing denser than the hard-sphere fcc crystal.

Nothing guarantees that the elo-like crystal for $0 \leq \kappa \lesssim 0.373$ and the bco-like crystal for $0.373 \lesssim \kappa \leq 1$ are the densest for lenses. Rather, taken together, these results suggest that lenses can take further advantage of their rotational degrees of freedom to achieve even higher densities than those we have reported thus far.

To further investigate this possibility, one could employ global optimization techniques to maximize the packing fraction under deforming fundamental cells; for example, the so-called adaptive-shrinking optimization scheme, which can be solved using either MC methods or other algorithms.[49] In Sec. III, a MC simulation procedure is described that we will employ to not only sketch the equilibrium phase behavior but also find even denser packings of lenses than the ones just described.

III. MONTE CARLO SIMULATION PROCEDURE

Monodisperse systems of lenses were investigated using MC method[68] in the isobaric-(isothermal) ensemble

(NPT).[75,76] Each lens is taken to have a surface area equal to $2\sigma^2$, with σ the unit of length. Each specific lens can be identified by the value of $R^* = R/\sigma$ or, equivalently, by θ or κ.[77]

To map out the phase diagram, from the low-density isotropic fluid to the high-density crystalline solid, in the κ—ϕ plane, we placed, for selected values of R^* in the range $[1/2\pi\ (\kappa = 1), 5\ (\kappa \simeq 0.056)]$, systems of N particles, with N in the range [100,1000], in a simulation box under periodic boundary conditions. The configurational coordinate of any lens is specified by the position of the particle center $\mathbf{r}$ and a unit vector $\hat{\mathbf{u}}$ along the particle C_∞ axis defining its orientation. The shape and size of the simulation box were allowed to vary under the action of a fixed pre-selected pressure p measured in units of k_BT/σ^3, with k_B the Boltzmann constant and T the temperature. The usage of a deformable, generally triclinic, box in a MC numerical technique to investigate crystalline phases and transitions between them is well-established.[78–80] The MC calculations were organized in cycles, each of them consisting on average of N trial translational moves, N trial rotational moves and one attempt to change the simulation box shape and size. The lens to translate or rotate was chosen randomly and such moves were accepted whenever no overlap resulted, the overlap criterion being based on the one that checks for overlap between two partial spherical surfaces.[61,65] Provided that it did not result in any overlap, the acceptance of a change to the shape and size of the simulation box was also subject to the corresponding Metropolis-like criterion depending on the value of p.[75,76] The maximal sizes of the various trials were adjusted before or after a calculation so as to have an acceptance probability of ∼30%, but never varied during a calculation so as not to violate the detailed balance condition. The random number generators used were either the Mersenne twister `mt19937`[81] or Numerical Recipe's `ran2`.[82] Usually, two sets of calculations were carried out depending on the initial configuration: in one set, lenses were initially arranged in an elo-like structure, while in the other set, lenses were initially arranged in a slightly expanded bco-like structure. The hcp-, fcc-like as well as the bco2-like structures were discarded as candidate crystal structures with which to start the MC-NPT numerical simulations on the following accounts. The hcp-like crystal is the least dense structure among the constructions described in Sec. II and preliminary calculations did confirm that it was not mechanically stable even at high p; the fcc-like crystal provides a packing fraction similar, though smaller than, the bco-like structure while the bco2-like crystal's sudden and unrecovered drop in the packing fraction suggests it may be a reasonable crystal structure only for large enough values of κ. Occasionally, compression runs starting from a configuration generated at a sufficiently low pressure in the isotropic fluid phase were also carried out (see supplementary material[100]). For any specific value of R^* and every value of p considered, equilibration runs lasted a minimum of 1×10^6 of MC steps and were followed by production runs of as many MC steps. During these runs, the average[83] of several quantities was computed including ϱ, measured in units of σ^{-3}, from which ϕ was obtained, and the nematic order parameter, S_2, calculated in the usual way[41,84] that also led to the individualisation of the nematic director $\hat{\mathbf{n}}$,[85] as well as a number, usually one thousand, of evenly sampled configurations were stored for subsequent analysis. The latter included the calculation of a large family of positional and orientational correlation functions. In particular, the center-to-center positional correlation function $g(r)$ defined as

$$g(r) = \frac{1}{\mathrm{N}} \left\langle \frac{1}{\varrho} \sum_{i=1}^{\mathrm{N}} \sum_{j \neq i}^{\mathrm{N}} \delta(r - r_{ij}) \right\rangle, \tag{1}$$

with $\langle\rangle$ indicating an ensemble average over configurations, $\delta(x)$ the usual radial Dirac delta function, and r_{ij} the distance separating the center of lenses i and j, and the second-order orientational correlation function $G_2^{\hat{\mathbf{u}}}(r)$ defined as

$$G_2^{\hat{\mathbf{u}}}(r) = \left\langle \frac{\sum_{i=1}^{\mathrm{N}} \sum_{j \neq i}^{\mathrm{N}} P_2(\hat{\mathbf{u}}_i \cdot \hat{\mathbf{u}}_j) \delta(r - r_{ij})}{\sum_{i=1}^{\mathrm{N}} \sum_{j \neq i}^{\mathrm{N}} \delta(r - r_{ij})} \right\rangle, \tag{2}$$

with $P_2(x)$ the second-order Legendre polynomial.

To improve on close packing density, dedicated MC-NPT numerical simulations were performed on systems with a very small number, N = 16, of particles whose relative scaled positions were kept fixed as in the bco-like crystal, only allowing for their orientations and the simulation box shape and size to vary subject to periodic boundary conditions. Similar to previous MC calculations, a cycle consisted of N attempted single-particle rotational moves and one attempted simulation box deformation though, differently from those MC calculations, allowance was made here for acceptance ratios as low as ∼1%. MC calculations of this type were run for several values of R^*. For any of these values, a few batches of calculations were carried out, each composed of (i) 10×10^6 cycle long MC calculations at $p\sigma^3/k_BT = 10^4$ starting from a slightly expanded bco-like configuration with all lenses aligned along the z axis; (ii) 10×10^6 cycle long MC calculations at $p\sigma^3/k_BT = 10^5$ starting from the last configuration generated in (i); (iii) 10×10^6 cycle long MC calculations at $p\sigma^3/k_BT = 10^6$ starting from the last configuration generated in (ii); (iv) 10×10^6 cycle long MC calculations at $p\sigma^3/k_BT = 10^6$ starting from the last configuration generated in (iii) during which averages were accumulated.

IV. MONTE CARLO SIMULATION RESULTS

A. Equilibrium phase behavior

By carrying out the above-described MC-NPT numerical simulations, the equation of state (EoS) was traced for several values of R^*. For each of the values of R^* considered, the various branches were identified by discontinuities in the EoS curve, the calculation of order parameters and positional and orientational correlation functions (examples of their graphs are provided in the supplementary material[100]) along with the direct visualization of snapshots of configurations generated during the MC runs.

For globular lenses, such as those with $R^* = 0.47$ and $\kappa \simeq 0.75$ [Fig. 7(a)], three phases could be distinguished: isotropic fluid, plastic solid,[86] and crystalline solid. The plastic character of the mid-dense phase, stable until $R^* \sim 0.5$ and $\kappa \sim 0.68$, was evidenced by the value of S_2 [Fig. 7(a)] together

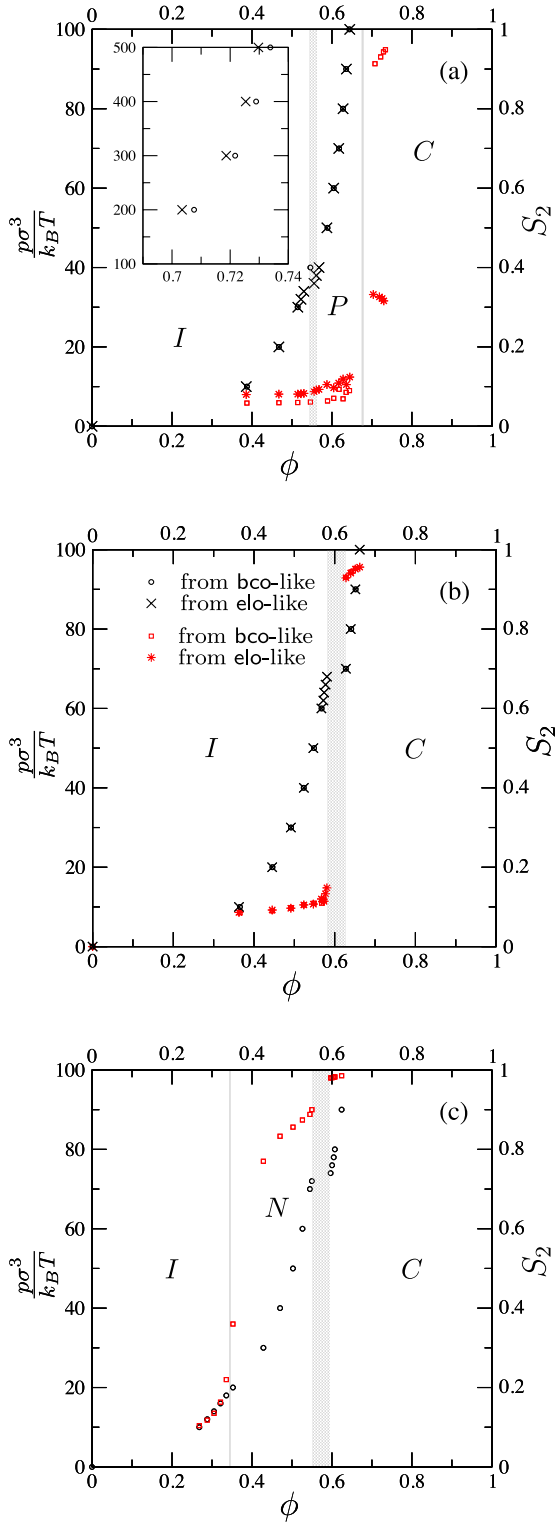

FIG. 7. Behavior of dimensionless pressure $p\sigma^3/k_BT$ (black crosses and circles; left ordinate axis) and nematic order parameter S_2 (red asterisks and squares; right ordinate axis) as a function of packing fraction ϕ (top and bottom abscissa axis) for a system with (a) $R^* = 0.47$ ($\kappa \simeq 0.75$) [inset zooms in on the high pressure region of the equation of state], (b) $R^* = 1/\sqrt{\pi}$ ($\kappa = 1/\sqrt{3}$), (c) $R^* = 1$ ($\kappa \simeq 0.29$). In the three panels, crosses and asterisks are for the sets of MC calculations starting from the elo-like structure while circles and squares are for the sets of MC calculations starting from the bco-like structure; error bars are within symbol size; I = isotropic, N = nematic, P = plastic, and C = crystal; gray thick lines or boxes approximately delimitate coexistent phases.

with the crystal-like character of $g(r)$. Provided that ϕ is sufficiently small and the system is in the isotropic fluid or plastic solid phases, essentially the same state point is reached irrespective of the type of initial configuration that is used. Discrepancies are instead seen at large values of ϕ [inset of Fig. 7(a)], with the state points obtained starting from the bco-like structure that maintain this type of organization while those obtained starting from the elo-like structure arresting in less dense, presumably metastable, states that appear to be the continuation of the plastic solid branch or defective crystals. For those states obtained starting from the elo-like structure, S_2 remains roughly constant, a bit larger than 0.25, the value that this quantity has in this initial configuration. Snapshots taken at certain values of p in the various phases and states are presented in Fig. 8.

Lenses neither globular nor flat, such as those with $R^* = 1/\sqrt{\pi}$ and $\kappa = 1/\sqrt{3} \simeq 0.58$ [Fig. 7(b)], exhibit two phases only: isotropic fluid and crystalline solid. No remnants are left of a plastic solid phase. The above-mentioned presumed metastability of the dense states reached starting from the elo-like structure was strongly suggested by the fact that, for values of R^* larger than 0.5 ($\kappa < 0.68$), initial configuration relatively rapidly and spontaneously evolved toward a bco-like crystal at sufficiently high p. For the system with $R^* = 1/\sqrt{\pi}$ ($\kappa = 1/\sqrt{3}$) as an example, Fig. 3 of the supplementary material[100] gives the evolution of ϕ and S_2 during the equilibration run at $p\sigma^3/k_BT = 70$ starting from a elo-like structure. These curves are compared to the evolution of the same quantities during the production run for the same system and at the same value of p whose corresponding equilibration run started from a bco-like structure. Observe that during this equilibration process, the simulation box passes from being orthorhombic to monoclinic. For these values of R^*, no discrepancies are seen in the EoS and S_2

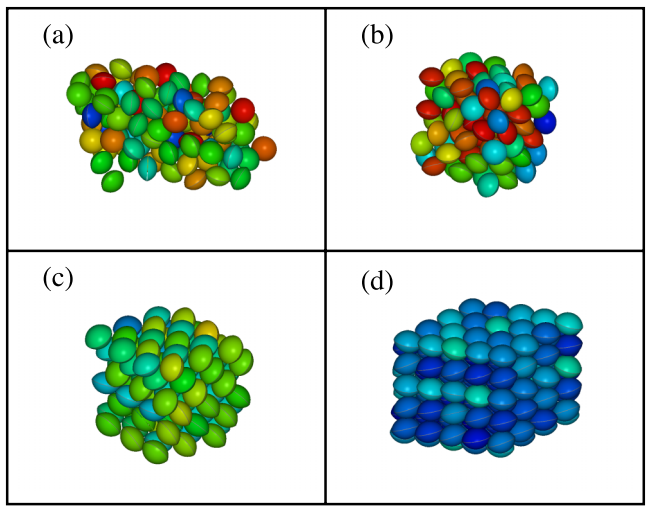

FIG. 8. Snapshots of configurations for the system with $R^* = 0.47$ ($\kappa \simeq 0.75$) taken at (a) $p\sigma^3/k_BT = 34$ in the isotropic fluid phase, (b) $p\sigma^3/k_BT = 70$ in the plastic solid phase, (c) $p\sigma^3/k_BT = 200$ in the defective crystal as obtained starting from an elo-like configuration, (d) $p\sigma^3/k_BT = 200$ in the crystal solid phase as obtained starting from a bco-like configuration. Particles were colored according to the angle their $\hat{\mathbf{u}}$ unit vector forms with the nematic director, with blue corresponding to 0° and red to 90°. The equatorial white "chord" helps to distinguish particle orientation. Images were created using the program QMGA.[69]

versus ϕ [Fig. 7(b)] curves, provided that p is sufficiently low so that the complete transformation of a elo-like configuration into a bco-like crystal is facilitated. Snapshots taken at certain values p in the isotropic fluid and crystalline solid phases are presented in Fig. 9. In the latter case, two snapshots are given, one obtained during the set of MC calculations that used an elo-like configuration as initial configuration and another obtained during the set of MC calculations that used a bco-like configuration as initial configuration.

For flat lenses, such as those with $R^* = 1$ and $\kappa \simeq 0.29$ [Fig. 7(c)], a (discotic) nematic liquid-crystalline phase intervenes between the isotropic fluid and crystal solid phases. The nematic character of the mid-dense phase, stable until the hard-infinitesimally thin-disk limit is reached,[87] was evidenced by the value of S_2 [Fig. 7(c)] together with the liquid-like character of $g(r)$. For flat lenses, only the MC-NPT numerical simulations starting from a bco-like structure were conducted. The aforementioned instability of the elo-like structure for non-globular lenses together with the similarity in packing fraction between this and the bco-like structure for sufficiently flat lenses indicated that there was no need to carry out the set of MC calculations starting from this structure. Snapshots taken at certain values of p in the various phases are presented in Fig. 10.

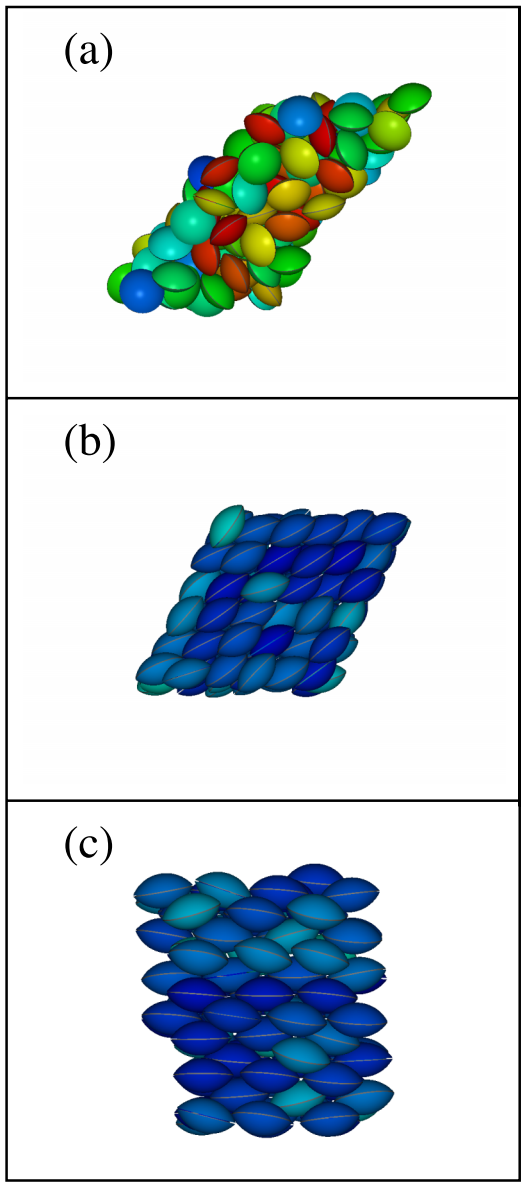

FIG. 9. Snapshots of configurations for the system with $R^* = 1/\sqrt{\pi}$ ($\kappa = 1/\sqrt{3}$) taken at (a) $p\sigma^3/k_BT = 68$ in the isotropic fluid phase, (b) $p\sigma^3/k_BT = 70$ in the crystal solid phase as obtained starting from an elo-like configuration, (c) $p\sigma^3/k_BT = 70$ in the crystal solid phase as obtained starting from a bco-like configuration. Particles were colored according to the angle their $\hat{\mathbf{u}}$ unit vector forms with the nematic director, with blue corresponding to 0° and red to 90°. The equatorial white "chord" helps to distinguish particle orientation. Images were created using the program QMGA.[69]

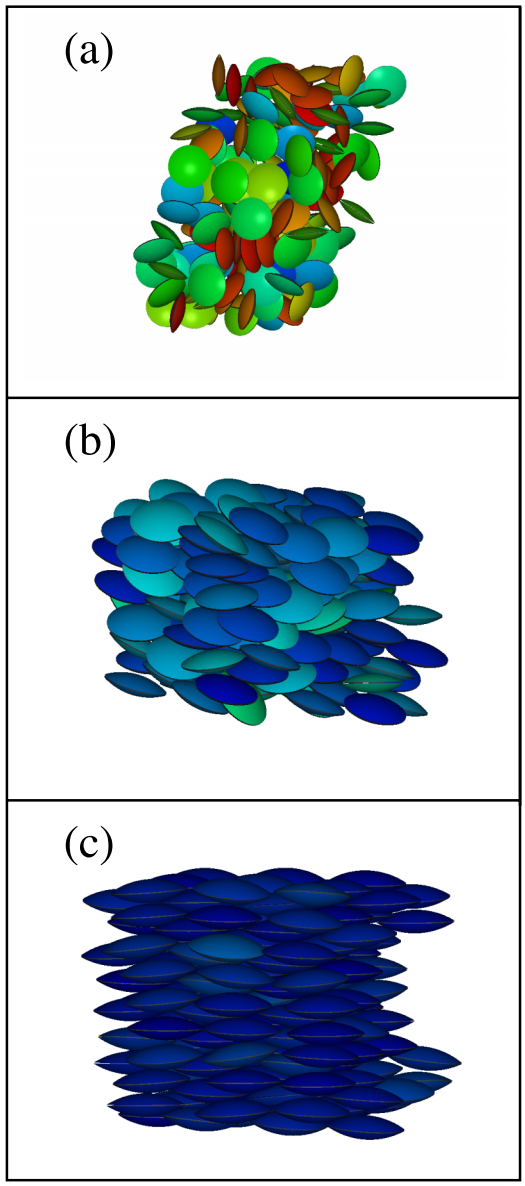

FIG. 10. Snapshots of configurations for the system with $R^* = 1$ ($\kappa \simeq 0.29$) taken at (a) $p\sigma^3/k_BT = 16$ in the isotropic fluid phase, (b) $p\sigma^3/k_BT = 50$ in the nematic liquid-crystal phase, (c) $p\sigma^3/k_BT = 90$ in the crystal solid phase. Particles were colored according to the angle their $\hat{\mathbf{u}}$ unit vector forms with the nematic director, with blue corresponding to 0° and red to 90°. The equatorial white "chord" helps to distinguish particle orientation. Images were created using the program QMGA.[69]

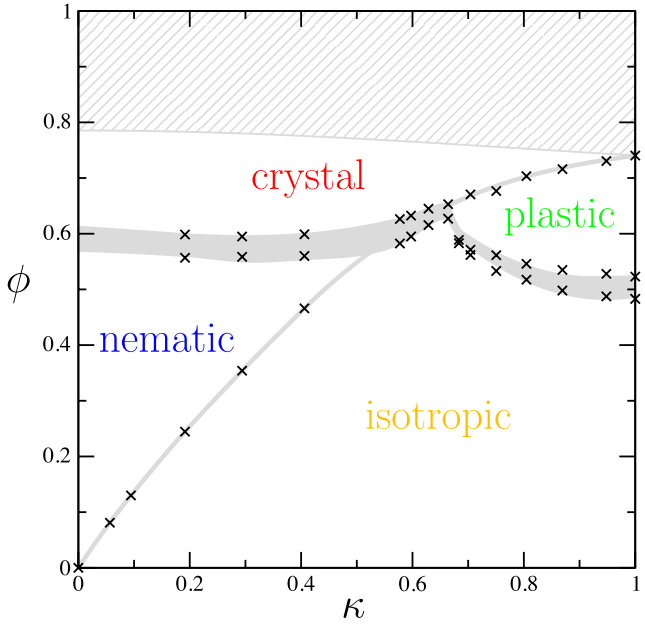

FIG. 11. Schematic phase diagram of lenses in the κ—ϕ plane.

By collecting all these MC data, a schematic phase diagram can be drawn (Fig. 11).[88] It very much resembles that of hard oblate ellipsoids.[32,38,39] This correspondence, while perhaps expected, between the two hard-particle phase diagrams extends to small and moderate values of ϕ, involving the presence of isotropic fluid, nematic liquid-crystalline and plastic solid phases[89] as well as the seeming absence of a columnar liquid-crystalline phase.[90] However, differences are apparent at larger values of ϕ within the crystalline solid region, especially toward the hard-sphere limit. In this limit, while hard oblate ellipsoids first form a fcc-like crystal,[38,39] and therefore require a successive phase transition on their way to reach the densest-known elo crystal,[39] globular lenses themselves tend to orient *quasi*-parallel also when packing most densely.

The MC-NPT numerical simulations carried out served to confirm that the densest packings of lenses are similar to the bco-like crystal construction devised in Section II. By using this structure as a starting point, the next objective is indeed the analytic calculation of the curve that bounds from below the hatched forbidden region in Fig. 11. This objective requires the intermediate step described in Section IV B and is achieved in Section V.

B. Denser packings

The mechanical stability of the bco-like crystal and its spontaneous formation starting from an elo-like structure observed in our MC calculations strongly indicate that the densest crystalline packing will likely resemble the bco-like crystal devised in Section II. In search for such a dense crystal, one has to assess more precisely the role played by the orientational order of the lenses and the shape and size of the fundamental cell.

This point was investigated by carrying out MC calculations with a very small number, N = 16, of particles at extremely high pressure. Table I summarizes the results obtained for these small-system-size high-pressure studies. One can see that there are two structural motifs that arise: either the fundamental cell retains its orthorhombic shape but pair of lenses tilt of the same angular amount in the opposite direction within the xz plane; or the lenses stay aligned but they collectively tilt within the xz plane within a fundamental cell that noticeably becomes monoclinic. Fig. 12 shows two snapshots taken for the case with $R^* = 0.49$ ($\kappa \simeq 0.70$) that respectively exemplify these two types of structures. From the values reported in Table I, the two structures appear to share very similar values of packing fraction and both are invariably denser than the bco-like crystal.

V. TOWARD THE DENSEST PACKINGS

The MC calculations described in Section IV B, carried out strongly compressing systems with a very small number of particles, suggest that a crystal denser than the bco-like crystal exists such that its structure is still body-centered-orthorhombic-like but the fundamental cell comprises two lenses. Their orientations are respectively described by the unit vectors $(\sin\pm\psi, 0, \cos\psi)$, with ψ the angle formed by the main symmetry axis of a lens with the z axis in Fig. 4 (inset of Table I). This crystal is denoted *tilted*-bco2-like. Guided by the MC calculations described in Section IV B, one can obtain for such a crystal an analytic expression of ϕ as a function of κ. By maximizing this expression with respect to ψ, the densest *tilted*-bco2-like crystal is obtained, the corresponding optimal angle ψ being labelled as $\psi_{\rm opt}$. The expressions for the optimal fundamental cell dimensions are

$$\mathrm{a} = \mathrm{a_x} = \sqrt{4R^2 - 4\left[\left(R - \frac{b}{2}\right)\cos\psi_{\rm opt}\right]^2} - 2\left(R - \frac{b}{2}\right)\sin\psi_{\rm opt}, \tag{3}$$

$$\mathrm{b} = \mathrm{b_z} = \sqrt{4R^2 - 4\left[\left(R - \frac{b}{2}\right)\sin\psi_{\rm opt}\right]^2} - 2\left(R - \frac{b}{2}\right)\cos\psi_{\rm opt}, \tag{4}$$

$$\mathrm{c} = \mathrm{c_y} = 2\sqrt{4R^2 - \frac{\mathrm{a_x}^2}{4} - \left[\frac{\mathrm{b_z}}{2} + 2\left(R - \frac{b}{2}\right)\cos\psi_{\rm opt}\right]^2}. \tag{5}$$

The MC calculations described in Section IV B also suggest that another crystal denser than the bco-like crystal may exist in which the lenses keep being aligned though tilted with respect to the z axis in Fig. 4 and the unit cell becomes monoclinic. This crystal is denoted *parallel*-mon-like crystal. Starting from the bco-like structure, tilting all the lenses by an angle $\psi_{\rm opt}$ leaves the value of a in Eq. (3) unchanged; setting the unit cell angle γ at the value

$$\gamma_{\rm opt} = \frac{\pi}{2} - \arctan\left[\frac{4\left(R - \frac{b}{2}\right)\sin\psi_{\rm opt}}{\mathrm{b_z}}\right], \tag{6}$$

makes $\mathrm{b}\sin\gamma_{\rm opt}$ equal to $\mathrm{b_z}$ in Eq. (4) and from this, the same value of $\mathrm{c} = \mathrm{c_y}$ as in Eq. (5) results. Consequently, the same maximal value of ϕ obtained for the *tilted*-bco2-like crystal is also attained by the *parallel*-mon-like crystal. That is, these two crystals, whose images are given in Figs. 13 and 14, are degenerate.

TABLE I. Results obtained from MC calculations for very small, N = 16, packings of lenses conducted at extremely high pressure. The inset gives a graphical definition of various quantities. Note that the angle ψ is positive (negative) when measured anticlockwise (clockwise) with respect to the z axis, while the edge c is along the y axis and α and β are, respectively, the angle between the b and c edges and the angle between the a and c edges.

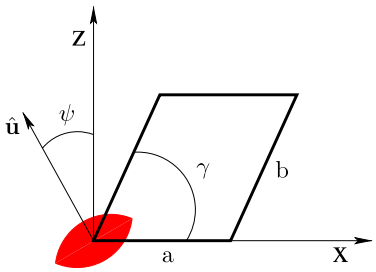

R^* (κ)	a/σ	c/σ	b/σ	α (deg)	β (deg)	γ (deg)	ϕ	ψ (deg)	S_2
0.40 (≃0.99)									
Batch I	0.798 70	1.129 48	0.795 99	90	90	90	0.740 79	±17.7	0.860
0.41 (≃0.95)									
Batch I	0.809 28	1.136 16	0.777 63	90	90	88.6	0.743 36	12.7	1.000
Batch II	0.806 82	1.138 42	0.778 01	90	90	90	0.743 55	±16.2	0.884
Batch III	0.805 99	1.139 17	0.778 23	90	90	90	0.743 63	±17.2	0.868
Batch IV	0.805 76	1.139 38	0.778 30	90	90	90	0.743 63	±17.7	0.863
Batch V	0.805 55	1.139 59	0.778 37	90	90	90	0.743 63	±17.7	0.856
0.43 (≃0.87)									
Batch I	0.845 26	1.133 36	0.740 53	90	90	89.0	0.744 19	3.1	1.000
Batch II	0.850 48	1.129 31	0.740 33	90	90	90	0.742 35	0.0	0.999
0.45 (≃0.80)									
Batch I	0.842 27	1.160 42	0.710 29	90	90	90	0.751 97	±12.9	0.943
Batch II	0.845 82	1.157 03	0.712 98	90	90	84.5	0.751 59	10.2	1.000
Batch III	0.846 16	1.156 71	0.712 87	90	90	84.6	0.751 56	10.1	1.000
Batch IV	0.844 99	1.157 81	0.713 27	90	90	84.4	0.751 69	10.4	1.000
Batch V	0.831 37	1.171 23	0.719 14	90	90	82.1	0.752 58	14.8	1.000
0.47 (≃0.75)									
Batch I	0.884 80	1.143 20	0.677 70	90	90	90	0.750 68	3.9	0.993
0.49 (≃0.70)									
Batch I	0.875 20	1.171 00	0.652 02	90	90	90	0.757 33	±10.0	0.967
Batch II	0.890 19	1.156 66	0.654 06	90	90	84.2	0.755 32	5.8	1.000
Batch III	0.883 17	1.163 27	0.651 26	90	90	90	0.756 37	±6.4	0.978
Batch IV	0.855 75	1.190 77	0.654 54	90	90	90	0.758 76	±11.9	0.934
0.51 (≃0.66)									
Batch I	0.942 30	1.128 51	0.624 86	90	90	89.9	0.747 75	±4.2	0.992
Batch II	0.943 39	1.125 75	0.624 24	90	90	89.7	0.749 44	±1.2	0.999
$1/\sqrt{\pi}$ ($1/\sqrt{3}$)									
Batch I	0.937 00	1.165 30	0.564 90	90	90	90	0.762 17	±7.0	0.992
Batch II	0.941 40	1.161 00	0.564 78	90	90	90	0.761 65	±5.1	0.994
Batch III	0.943 74	1.158 80	0.568 81	90	90	83.1	0.761 30	3.5	1.000
Batch IV	0.944 45	1.158 10	0.568 60	90	90	83.3	0.761 23	3.4	1.000
1.00 (≃0.29)									
Batch I	1.066 00	1.144 20	0.318 33	90	90	90	0.776 01	±0.8	1.000
Batch II	1.065 91	1.144 56	0.320 21	90	90	84.0	0.775 83	0.6	1.000
Batch III	1.017 65	1.356 33	0.345 56	90	90	67.2	0.778 20	2.3	1.000

The degree of degeneracy is however not limited to being twofold: it is actually infinite. In fact, taking laminae of the *tilted*-bco2- and *parallel*-mon-like crystals, one can stack them at will, regularly or irregularly, to generate an infinite set of dense packings all having the same maximal value of ϕ. Fig. 15 provides an example of such a stacking. Let the first layer be arranged in the plane xy. Note that inasmuch a single layer is concerned, there is no difference between the *tilted*-bco2- and *parallel*-mon-like crystals. Differences appear because of the way the next layer is arranged. Suppose that this is set on top of the first along the z axis as in a *tilted*-bco2-like crystal. Then the third layer is arranged again as in a *tilted*-bco2-like crystal. Now the fourth layer is instead set as in a *parallel*-mon-like crystal. This process is repeated uninterruptedly always with the possibility to choose to arrange the layers in either of the two ways.

The two *tilted*-bco2- and *parallel*-mon-like crystals, together with their, generally non-periodic, stacking variants are presently the densest-known packings for lenses. Fig. 16 provides the curve of ϕ vs. κ for such dense ordered packings, compared to the corresponding curve for the bco-like crystal. The non-lattice orthorhombic packing, the lattice monoclinic packing, and their stacking variants improve a little yet significantly on the "parent" lattice orthorhombic packing. While the latter's ϕ grows smoothly as κ is decreased from unity, the formers' ϕ grows steeply (linearly). The two curves tend to merge toward the hard-infinitesimally thin-disk limit. In fact, for $\kappa \to 0$ the value of ψ_{opt} tends to 0, i.e., flat lenses progressively tend to arrange perfectly parallel to one another in the new *tilted*-bco2-like crystal, as they do in the bco-like crystal; or they progressively tend to arrange perfectly perpendicularly to the z axis in Fig. 4 in the new

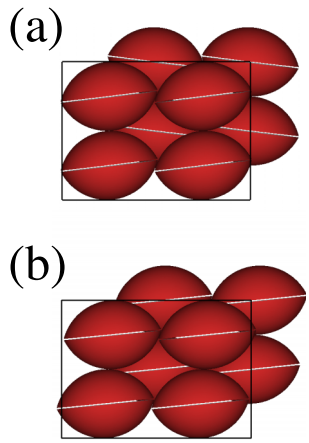

FIG. 12. Snapshots taken for the case with $R^* = 0.49$ ($\kappa \simeq 0.70$) as examples of the orthorhombic (a) and monoclinic (b) structures obtained in the small-system-size high-pressure MC calculations. What are shown are front views. That is why only the 8 lenses at the front are seen, each of the other 8 at the rear being just behind. The black rectangular box is there to give a visual impression of the simulation box geometry: note that in part (a) the equators of the lenses are touching the vertical edges while in part (b) two lenses have their equators beyond and other two within the vertical edges. Lenses were all colored in red. The white "chords" separating the two spherical caps of a lens are there to give a visual impression of the orientational pattern adopted. Images were created with the program QMGA.[69]

parallel-mon-like crystal, again as they do in the bco-like crystal. This is evidenced by Fig. 17 whose part (a) provides the dependence of ψ_{opt} as a function of κ and part (b) that of γ_{opt} as a function of κ. In the hard-sphere limit ψ_{opt} approaches the value ~18°; then it decreases *quasi*-linearly as κ decreases. Starting from a value of 90° in the hard-sphere limit, the value of γ_{opt} decreases as the lenses flatten until vanishing in the hard-infinitesimally thin-disk limit.

The limiting values reached by the fundamental cell dimensions and the angles ψ_{opt} and γ_{opt} as $\kappa \to 0$ are

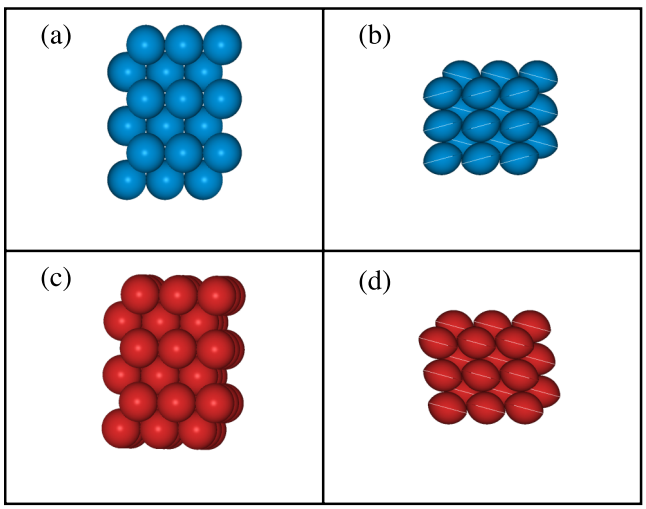

FIG. 13. Images of the *tilted*-bco2- ((a) and (b)) and *parallel*-mon-like ((c) and (d)) crystals, created using the program QMGA.[69] They are for $R^* = 0.45$ ($\kappa \simeq 0.80$). In cases (a) and (b), lenses are colored according to the angle their $\hat{\mathbf{u}}$ unit vector forms with the nematic director (axis z) with blue corresponding to 0° and red to 90° while in cases (c) and (d) are all colored in red. The equatorial white "chord" helps to distinguish particle orientation.

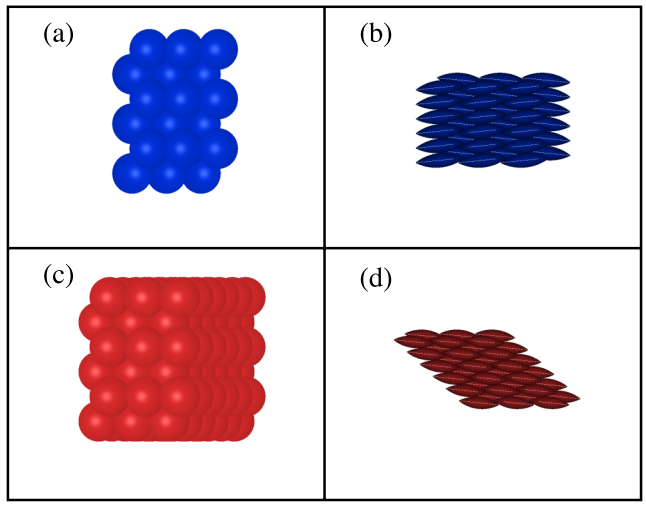

FIG. 14. Images of the *tilted*-bco2- ((a) and (b)) and *parallel*-mon-like ((c) and (d)) crystals, created using the program QMGA.[69] They are for $R^* = 1$ ($\kappa \simeq 0.29$). In cases (a) and (b), lenses are colored according to the angle their $\hat{\mathbf{u}}$ unit vector forms with the nematic director (axis z) with blue corresponding to 0° and red to 90° while in cases (c) and (d) all are colored in red. The equatorial white "chord" helps to distinguish particle orientation.

consistent with both the *tilted*-bco2-like and *parallel*-mon-like crystals tending to have a flatter fundamental cell in which the lenses tend to assume an in-layer square arrangement (e.g., $b_z \to 0$ and $a_x \simeq c_y$) rather than a hexagonal columnar arrangement. This would seem to contradict the argument that hard-infinitesimally thin disks form a (infinitely pressure) hexagonal columnar phase.[91] Rather, results in that limit appear to depend substantially on the way that limit is approached, i.e., on details of the hard disk-like particle chosen to approach the hard-infinitesimally thin disk. If that particle is a hard cut-sphere, a system of which forms a hexagonal columnar phase already when particles are finitely thick,[45] the same liquid-crystalline phase appears to persist all the way to the hard-infinitesimally thin-disk limit. If that particle is a hard oblate ellipsoid or lens, similar extrapolations cannot be made.

Compared to hard oblate ellipsoids arranged in their densest-known configuration,[35] the *tilted*-bco2-like and *parallel*-mon-like crystals and their stacking variants are

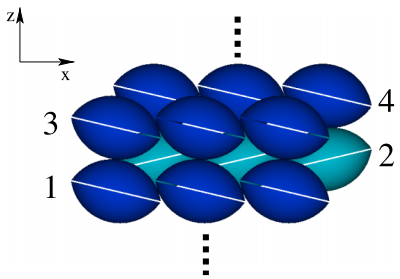

FIG. 15. Example of a dense ordered packing obtained by stacking at will along the z axis laminae of either the *tilted*-bco2- and *parallel*-mon-like crystals extending on the xy plane. Particles are colored according to the sign of the angle their $\hat{\mathbf{u}}$ unit vector forms with the axis z, light (dark) blue if positive (negative). The equatorial white "chord" helps to distinguish particle orientation. Images were created using the program QMGA.[69]

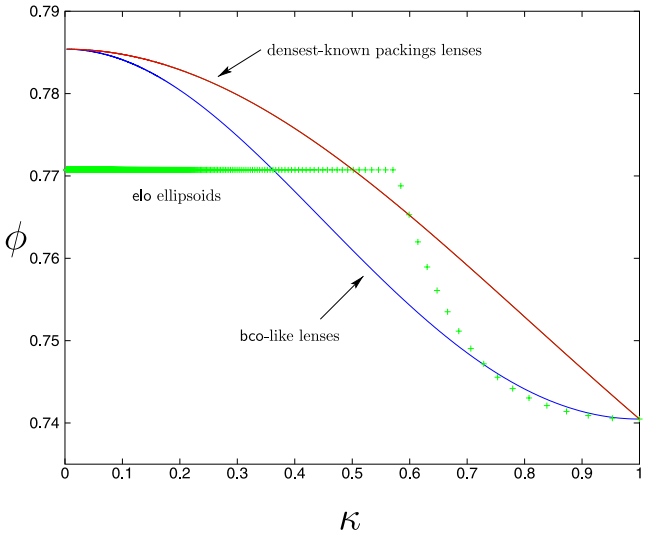

FIG. 16. Packing fraction ϕ as a function of the aspect ratio κ for the bco-like crystal (blue line) and the *tilted*-bco2-like and *parallel*-mon-like crystals and their stacking variants (red line) of lenses and for the elo crystal of hard oblate ellipsoids (green pluses).

denser throughout the whole range of κ except in a small "pocket" around $\kappa \sim 1/\sqrt{3}$ where the hard oblate ellipsoid ϕ curve has a kink.

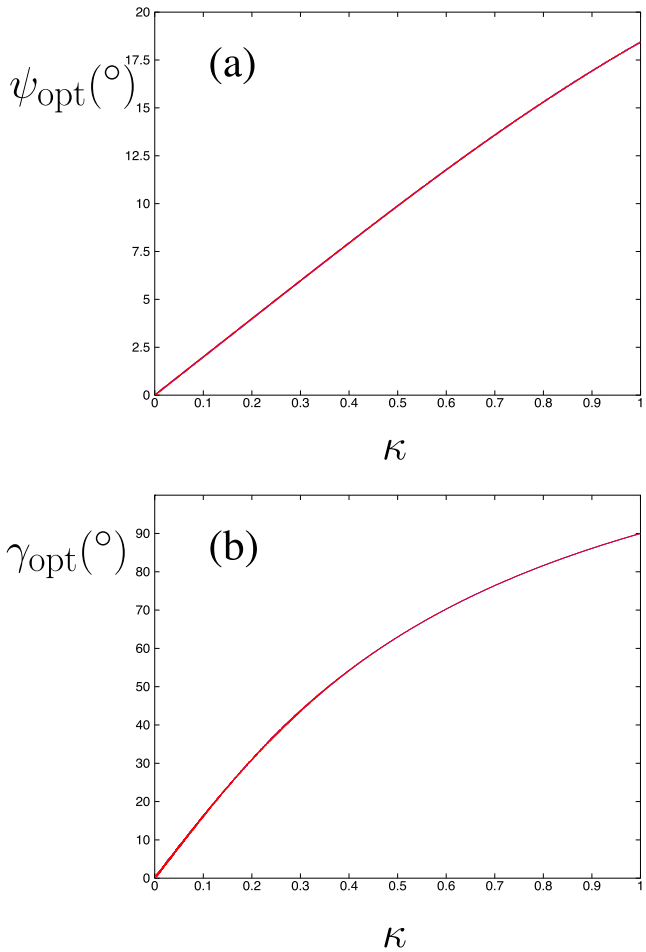

FIG. 17. (a) The optimal angle ψ_{opt} as a function of the aspect ratio κ for *tilted*-bco2-like crystals of lenses. (b) The optimal angle γ_{opt} as a function of the aspect ratio κ for *parallel*-mon-like crystals of lenses.

VI. CONCLUSIONS

By using both theoretical and computational techniques, this work investigates dense ordered packings and equilibrium phase behavior of hard convex lens-shaped particles or lenses. These hard particles are defined as the volume common to two intersecting congruent spheres, thus being seemingly similar to hard oblate ellipsoids. This work has proceeded in three steps: first, the analytic constructions of several dense packings; then, the usage of Monte Carlo method to both sketch the phase diagram, qualitatively very similar to that of hard oblate ellipsoids, and guide toward denser packings; finally, the analytic constructions of these denser packings. They consist of two, interestingly degenerate, crystals, a non-lattice orthorhombic one with a two-particle basis and a lattice monoclinic one, together with their, regular or irregular, stacked laminations. With the proviso that the existence of even denser, e.g., multiparticle-basis periodic, packings cannot be excluded, these two crystals and their infinitely degenerate stacking variants are currently the hard convex lens-shaped particle densest-known packings. Organizing principles were devised[92] to guide one to ascertain the densest packings of hard convex or concave particles. Our densest packing constructions are consistent with the specific organizing principle stated there that "the densest packings of hard congruent centrally symmetric particles that do not possess three equivalent principal axes can be non-(Bravais)-lattices." In spite of a seemingly similar shape and an overall very similar phase diagram, the dense packing characteristics of hard convex lens-shaped particles differ from those of hard oblate ellipsoids. They share more in common with hard-sphere (Barlow) degenerate densest packings.

Previously, degenerate, generally non-periodic, crystals were observed for di- and n-mers of hard disks and spheres[93,94] while a degenerate quasicrystal-like structure has been reported for hard triangular bipyramids.[95] While it is easy to imagine the degeneracy of hard sphere di- and n-mers positionally ordered packings, by pairing or more generally linking randomly hard-sphere monomers arranged in their densest fcc or hcp crystal packings or their (Barlow) stacking variants, more remarkable is the observation of the degeneracy in the quasicrystal-like structure of hard triangular bipyramids, as it was not straightforward to envision that pairing tetrahedra into triangular bipyramids did not affect the quasicrystal-like structure. In the conclusions of that work, it was also hypothesized that degenerate dense packings might be common in systems made of hard dimers. While viewing a hard convex lens-shaped particle as a dimer of hard convex spherical-cap body particles is certainly consistent with such a hypothesis, the set of degenerate dense packings of hard convex lens-shaped particles nonetheless constitutes a new class. In fact, they are obtained starting from two different, themselves degenerate, crystals rather than pairing into dimers a previously characterized monomer arrangement.[96,97]

Concerning possible ways to continue this work, one could mention three. It would be interesting to conduct a similar study on the rod-like analogues of the disk-like particles considered herein, namely, those hard spindle-shaped particles generated by rotating a circular arc around its

subtended chord. Further attention would be deserved to rigorously assessing the respective thermodynamic stability of the two hard convex lens-shaped particle crystals, in much the same way as done for the hard-sphere fcc and hcp crystals.[29,98] Perhaps the most direct continuation of this work is however an extensive study on dense disordered packings of hard convex lens-shaped particles that will explore the potentiality of these model colloidal particles to be particularly good glass formers, combining as they do non-spherical shape[99] with degeneracy in the dense packings.

ACKNOWLEDGMENTS

We are grateful to Yang Jiao for insightful remarks about the manuscript. We thank an anonymous referee for asking us to take a closer look at the isotropic-to-nematic phase transition behavior in the hard infinitesimally thin-disk limit. G.C. thanks the Government of Spain for the award of a Ramón y Cajal research fellowship and the financial support under the Grant No. FIS2013-47350-C5-1-R. S.T. was supported by the U.S. National Science Foundation under Grant Nos. DMR-0820341 and DMS-1211087.

[1]L. Fejes Tóth, *Regular Figures* (Pergamon Press, Oxford, 1964).
[2]C. A. Rogers, *Packing and Covering* (Cambridge University Press, Cambridge, 1964).
[3]J. H. Conway and N. J. A. Sloane, *Sphere Packing, Lattices and Groups* (Springer-Verlag, New York, 1999).
[4]P. Brass, W. Moser, and J. Pach, *Research Problems in Discrete Geometry* (Springer-Verlag, New York, 2005).
[5]T. Aste and D. Weaire, *The Pursuit of Perfect Packing* (Taylor & Francis, New York, 2008).
[6]P. M. Chaikin and T. C. Lubensky, *Principles of Condensed Matter Physics* (Cambridge University Press, Cambridge, 1995).
[7]W. D. Callister, *Fundamentals of Materials Science and Engineering* (John Wiley & Sons, New York, 2001).
[8]S. Torquato, *Random Heterogeneous Materials* (Springer-Verlag, New York, 2002).
[9]N. W. Ashcroft and N. D. Mermin, *Solid State Physics* (Cengage Learning, Belmont, 1976).
[10]G. Grosso and G. Pastori Parravicini, *Solid State Physics* (Academic Press, San Diego, 2000).
[11]R. Zallen, *The Physics of Amorphous Solids* (Wiley VCH, Weinheim, 2004).
[12]P. G. de Gennes and J. Prost, *The Physics of Liquid Crystals* (Clarendon Press, Oxford, 1993).
[13]J. A. Barker and D. Henderson, Rev. Mod. Phys. **48**, 587 (1976).
[14]N. H. March and M. P. Tosi, *Introduction to Liquid State Physics* (World Scientific, Singapore, 2002).
[15]W. B. Russel, D. A. Saville, and W. R. Schowalter, *Colloidal Dispersions* (Cambridge University Press, Cambridge, 1989).
[16]S. C. Glotzer and M. J. Solomon, Nat. Mater. **6**, 557 (2007).
[17]M. J. Solomon, Curr. Opin. Colloid Interface Sci. **16**, 158 (2011).
[18]S. Sacanna, D. J. Pine, and G. R. Yi, Soft Matter **9**, 8096 (2013).
[19]*Theory and Simulation of Hard-Sphere Fluids and Related Systems*, edited by A. Mulero, Lecture Notes in Physics Vol. 753 (Springer, Berlin, 2008).
[20]G. Parisi and F. Zamponi, Rev. Mod. Phys. **82**, 789 (2010).
[21]S. Torquato and F. H. Stillinger, Rev. Mod. Phys. **82**, 2633 (2010).
[22]J. G. Kirkwood, J. Chem. Phys. **7**, 919 (1939).
[23]W. W. Wood and J. D. Jacobson, J. Chem. Phys. **27**, 1207 (1957).
[24]B. J. Alder and T. E. Wainwright, J. Chem. Phys. **27**, 1208 (1957).
[25]W. G. Hoover and F. H. Ree, J. Chem. Phys. **49**, 3609 (1968).
[26]M. D. Rintoul and S. Torquato, Phys. Rev. Lett. **77**, 4198 (1996); J. Chem. Phys. **105**, 9258 (1996).
[27]S. Torquato, T. M. Truskett, and P. G. Debenedetti, Phys. Rev. Lett. **84**, 2064 (2000).
[28]L. V. Woodcock, Nature **385**, 141 (1997); **388**, 236 (1997).
[29]S. C. Mau and D. A. Huse, Phys. Rev. E **59**, 4396 (1999).
[30]T. C. Hales, Ann. Math. **162**, 1063 (2005).
[31]J. W. Perram, M. S. Wertheim, J. L. Lebowitz, and G. O. Williams, Chem. Phys. Lett. **105**, 277 (1984); J. W. Perram and M. S. Wertheim, J. Comput. Phys. **58**, 409 (1985).
[32]D. Frenkel, B. M. Mulder, and J. P. McTague, Phys. Rev. Lett. **52**, 287 (1984); D. Frenkel and B. M. Mulder, Mol. Phys. **55**, 1171 (1985).
[33]M. P. Allen and C. P. Mason, Mol. Phys. **86**, 467 (1995); P. J. Camp, C. P. Mason, M. P. Allen, A. A. Khare, and D. A. Kofke, J. Chem. Phys. **105**, 2837 (1996); P. J. Camp and M. P. Allen, *ibid.* **106**, 6681 (1997).
[34]A. Donev, I. Cisse, D. Sachs, E. A. Variano, F. H. Stillinger, R. Connelly, S. Torquato, and P. M. Chaikin, Science **303**, 990 (2004).
[35]A. Donev, F. H. Stillinger, P. M. Chaikin, and S. Torquato, Phys. Rev. Lett. **92**, 255506 (2004).
[36]W. Man, A. Donev, F. H. Stillinger, M. T. Sullivan, W. B. Russel, D. Heeger, S. Inati, S. Torquato, and P. M. Chaikin, Phys. Rev. Lett. **94**, 198001 (2005).
[37]A. Donev, S. Torquato, and F. H. Stillinger, J. Comput. Phys. **202**, 737 (2005); **202**, 765 (2005).
[38]P. Pfleiderer and T. Schilling, Phys. Rev. E **75**, 020402 (2007); M. Radu, P. Pfleiderer, and T. Schilling, J. Chem. Phys. **131**, 164513 (2009).
[39]G. Odriozola, J. Chem. Phys. **136**, 134505 (2012); G. Bautista-Carvajal, A. Moncho-Jordá, and G. Odriozola, *ibid.* **138**, 064501 (2013).
[40]L. Onsager, Ann. N. Y. Acad. Sci. **51**, 627 (1949).
[41]J. Vieilliard-Baron, Mol. Phys. **28**, 809 (1974).
[42]D. W. Rebertus and K. M. Sando, J. Chem. Phys. **67**, 2565 (1977).
[43]M. Hosino, H. Nakano, and H. Kimura, J. Phys. Soc. Jpn. **46**, 1709 (1979); **47**, 740 (1979).
[44]D. Frenkel, J. Phys. Chem. **91**, 4912 (1987); D. Frenkel, H. N. W. Lekkerkerker, and A. Stroobants, Nature **332**, 822 (1988); P. Bolhuis and D. Frenkel, J. Chem. Phys. **106**, 666 (1997).
[45]J. A. C. Veerman and D. Frenkel, Phys. Rev. A **45**, 5632 (1990).
[46]P. D. Duncan, M. Dennison, A. J. Masters, and M. R. Wilson, Phys. Rev. E **79**, 031702 (2009); P. D. Duncan, A. J. Masters, and M. R. Wilson, *ibid.* **84**, 011702 (2011).
[47]J. H. Conway and S. Torquato, Proc. Natl. Acad. Sci. U. S. A. **103**, 10612 (2006).
[48]E. R. Chen, Discrete Comput. Geom. **40**, 214 (2008).
[49]S. Torquato and Y. Jiao, Nature **460**, 876 (2009); Phys. Rev. E **80**, 041104 (2009).
[50]A. Haji-Akbari, M. Engel, A. S. Keys, X. Zheng, R. G. Petschek, P. Palffy-Muhoray, and S. C. Glotzer, Nature **462**, 773 (2009).
[51]A. Jaoshvili, A. Esakia, M. Porrati, and P. M. Chaikin, Phys. Rev. Lett. **104**, 185501 (2010).
[52]Y. Kallus, V. Elser, and S. Gravel, Discrete Comput. Geom. **44**, 245 (2010).
[53]E. R. Chen, M. Engel, and S. C. Glotzer, Discrete Comput. Geom. **44**, 253 (2010).
[54]S. Torquato and Y. Jiao, Phys. Rev. E **81**, 041310 (2010).
[55]Y. Jiao and S. Torquato, Phys. Rev. E **84**, 041309 (2011).
[56]U. Agarwal and F. A. Escobedo, Nat. Mater. **10**, 230 (2011).
[57]Y. Jiao and S. Torquato, J. Chem. Phys. **135**, 151101 (2011); D. Chen, Y. Jiao, and S. Torquato, J. Phys. Chem. B **118**, 7981 (2014).
[58]P. F. Damasceno, M. Engel, and S. C. Glotzer, ACS Nano **6**, 609 (2012); P. F. Damasceno, M. Engel, and S. C. Glotzer, Science **337**, 453 (2012).
[59]Y. Jiao, F. H. Stillinger, and S. Torquato, Phys. Rev. E **79**, 041309 (2009); **81**, 041304 (2010); R. D. Batten, F. H. Stillinger, and S. Torquato, *ibid.* **81**, 061105 (2010).
[60]P. J. Camp, M. P. Allen, and A. J. Masters, J. Chem. Phys. **111**, 9871 (1999).
[61](a) G. Cinacchi and J. S. van Duijneveldt, J. Phys. Chem. Lett. **1**, 787 (2010); (b) G. Cinacchi, J. Chem. Phys. **139**, 124908 (2013); (c) G. Cinacchi and A. Tani, *ibid.* **141**, 154901 (2014).
[62](a) E. Frezza, A. Ferrarini, H. B. Kolli, A. Giacometti, and G. Cinacchi, J. Chem. Phys. **138**, 164906 (2013); (b) H. B. Kolli, E. Frezza, G. Cinacchi, A. Ferrarini, A. Giacometti, and T. S. Hudson, *ibid.* **140**, 081101 (2014); (c) H. B. Kolli, E. Frezza, G. Cinacchi, A. Ferrarini, A. Giacometti, T. S. Hudson, C. De Michele, and F. Sciortino, Soft Matter **10**, 8171 (2014).
[63]R. Gabbrielli, Y. Jiao, and S. Torquato, Phys. Rev. E **89**, 022133 (2014).
[64]Note that in Refs. 61(a) and 61(c), where hard (hollowed) spherical caps of small curvature were studied, they too were simply called (contact-) lens–like particles.
[65]M. He and P. Siders, J. Phys. Chem. **94**, 7280-7288 (1990).
[66]A. Baule, R. Mari, L. Bo, L. Portal, and H. A. Makse, Nat. Commun. **4**, 2194 (2013).
[67]For example by the method developed by: S. Sacanna, M. Korpics, K. Rodriguez, L. Colón-Meléndez, S. H. Kim, D. J. Pine, and G. R. Yi, Nat. Commun. **4**, 1688 (2013).

[68]N. Metropolis, A. W. Rosenbluth, M. N. Rosenbluth, A. H. Teller, and E. Teller, J. Chem. Phys. **21**, 1087 (1953).
[69]A. T. Gabriel, T. Meyer, and G. Germano, J. Chem. Theory Comput. **4**, 468 (2008), http://qmga.sourceforge.net.
[70]E. Bain, Trans. Am. Inst. Min. Metall. Eng. **70**, 25-35 (1924).
[71]One beautiful recent example of Bain transformations is provided by superlattices of PbSe nanocrystals: Z. Quan, D. Wu, J. Zu, W. H. Evers, J. M. Boncella, L. D. A. Siebbeles, Z. Wang, A. Navrotsky, and H. Xu, Proc. Natl. Acad. Sci. U. S. A. **111**, 9054-9057 (2014).
[72]The volume of a lens is that common to two intersecting congruent spheres. In terms of the radius R and opening angle θ it is $v = \frac{2\pi}{3}R^3\left(2 - 3\cos\frac{\theta}{2} + \cos^3\frac{\theta}{2}\right)$. The volume of an oblate ellipsoid with the same major and minor axes is instead $v = \frac{4\pi}{3}R^3\left(1 - \cos\frac{\theta}{2} - \cos^2\frac{\theta}{2} + \cos^3\frac{\theta}{2}\right)$.
[73]M. Gardner, *The Colossal Book of Mathematics* (Norton, New York, 2001).
[74]Y. Kallus, Adv. Math. **264**, 355-370 (2014).
[75]W. W. Wood, J. Chem. Phys. **48**, 415 (1968); **52**, 729 (1970).
[76]M. P. Allen and D. J. Tildesley, *Computer Simulation of Liquids* (Clarendon Press, Oxford, 1987).
[77]Note that $\cos\frac{\theta}{2} = 1 - 1/\left(2\pi R^{*2}\right)$ and that $\kappa = \frac{1-\cos\frac{\theta}{2}}{\sin\frac{\theta}{2}}$.
[78]R. Najafabadi and S. Yip, Scr. Metall. **17**, 1199 (1983).
[79]S. Yashonath and C. N. R. Rao, Mol. Phys. **54**, 245 (1985).
[80]P. A. Monson and D. A. Kofke, Adv. Chem. Phys. **115**, 113 (2000).
[81]M. Matsumoto and T. Nishimura, ACM Trans. Model. Comput. Simul. **8**, 3 (1998).
[82]W. H. Press, S. A. Teukolsky, W. T. Vetterling, and B. P. Flannery, *Numerical Recipes: The Art of Scientific Computing* (Cambridge University Press, Cambridge, 1996).
[83]Error bars on these averages were estimated using the block method described by H. Flyvbjerg and H. G. Petersen, J. Chem. Phys. **91**, 461 (1989).
[84]R. D. Mountain and T. W. Rijgrok, Physica A **89**, 522 (1977).
[85]Note that $\hat{\mathbf{n}}$, as defined as the eigenvector corresponding to the largest eigenvalue, i.e., S_2, of the $\mathbf{Q}$ order tensor,[84] keeps being defined in any, including effectively isotropic, finite-size system.
[86]This is a solid phase, also called rotator phase, in which particle positions are regularly arranged as in a crystal but orientations are instead isotropically distributed.
[87](a) D. Frenkel and R. Eppenga, Phys. Rev. Lett. **49**, 1089 (1982); (b) R. Eppenga and D. Frenkel, Mol. Phys. **52**, 1303 (1984); (c) G. Cinacchi and A. Tani, J. Phys. Chem. B **119**, 5671 (2015).
[88]More precise phase boundaries could be obtained by performing free-energy calculations via thermodynamic integration. These calculations, possible whenever candidate equilibrium phases are known and the overall phase diagram mapped out, are not considered here. One could also apply replica-exchange Monte Carlo methods, as was done for hard ellipsoids,[39] which may be the subject of a future work.
[89]It may be of interest to investigate how the boundaries of the isotropic-to-nematic and plastic-to-crystal phase transitions approach respectively the limits $\kappa \to 0$ and $\kappa \to 1$. This point is elaborated in the supplementary material.[100]
[90]Note that the argument that attempts to rationalize the absence of a columnar phase in a system of freely rotating hard oblate ellipsoids (as well as that of a smectic phase in a freely rotating hard prolate ellipsoid system) in terms of the affine transformation that relates a single hard ellipsoid to a hard sphere or a system of aligned hard ellipsoids to a system of hard spheres cannot be applied to lenses as that affine transformation does not hold for them.
[91]M. Bates and D. Frenkel, Phys. Rev. E **57**, 4824 (1998).
[92]Y. Jiao and S. Torquato, Phys. Rev. E **86**, 011102 (2012).
[93](a) K. W. Wojciechowski, D. Frenkel, and A. C. Branká, Phys. Rev. Lett. **66**, 3168 (1991); (b) C. Vega, E. P. A. Paras, and P. A. Monson, J. Chem. Phys. **96**, 9060 (1992); (c) A. P. Malanoski and P. A. Monson, *ibid.* **107**, 6899 (1997).
[94]N. C. Karayiannis, K. Foteinopoulou, and M. Laso, Phys. Rev. Lett. **103**, 045703 (2009); N. C. Karayiannis, K. Foteinopoulou, C. F. Abrams, and M. Laso, Soft Matter **6**, 2160 (2010).
[95]A. Haji-Akbari, M. Engel, and S. C. Glotzer, Phys. Rev. Lett. **107**, 215702 (2011).
[96]Rather, the converse might be stated for lenses. Their arrangements *a fortiori* constitute dense ordered packings also for hard convex spherical-cap body particles (only those that have the pole of the spherical part distant from the basal disk less than the sphere radius, i.e., having an aspect ratio χ^* as defined elsewhere[97] such that $0 < \chi^* \leq \frac{1}{2}$) once these have been paired into hard convex lens-shaped particles. However, these arrangements are not necessarily the densest, as the example of semicircles in two dimensions shows.[4]
[97]C. Avendaño, C. M. Liddell Watson, and F. A. Escobedo, Soft Matter **9**, 9153 (2013).
[98]E. G. Noya and N. G. Almarza, Mol. Phys. **113**, 1061 (2015).
[99]The propensity of monodisperse systems of hard non-spherical particles to form glasses has been explored before, e.g., P. Pfleiderer, K. Milinkovic, and T. Schilling, Europhys. Lett. **84**, 16003 (2008).
[100]See supplementary material at http://dx.doi.org/10.1063/1.4936938 for more details on the dense packing constructions in Sec. II and on the equilibrium phase behavior in Sec. IV A.